Received: 4 November 2022 | Revised: 12 January 2023 | Accepted: 10 February 2023

IET Communications

DOI: 10.1049/cmu2.12592

The Institution of Engineering and Technology WILEY

ORIGINAL RESEARCH

Maximizing the network outage rate for fast fluid antenna multiple access systems

Kai-Kit Wong[1] | **Kin-Fai Tong**[1] | **Yu Chen**[2] | **Yangyang Zhang**[3]

[1]Department of Electronic and Electrical Engineering, University College London, London, UK

[2]School of Information and Communication Engineering (SICE), Beijing University of Posts and Telecommunications, Beijing, China

[3]Kuang-Chi Science Limited, Hong Kong SAR, China

Correspondence
Kai-Kit Wong, Department of Electronic and Electrical Engineering, University College London, London, UK.
Email: kai-kit.wong@ucl.ac.uk

Funding information
Engineering and Physical Sciences Research Council, Grant/Award Number: EP/W026813/1; National Natural Science Foundation of China, Grant/Award Number: 61901055

Abstract

Using reconfigurable fluid antennas, it is possible to have a software-controlled position-tuneable antenna to realize spatial diversity and multiplexing gains that are previously only possible using multiple antennas. Recent results illustrated that fast fluid antenna multiple access (f-FAMA) which always tunes the antenna to the position for maximum signal-to-interference ratio (SIR) on a symbol-by-symbol basis, could support hundreds of users on the same radio channel, all by a single fluid antenna at each user without complex coordination and optimization. The network outage rate, nevertheless, depends on the SIR threshold chosen for each user. Motivated by this, this paper adopts a first-order approximation to obtain the outage probability expression from which a closed-form solution is derived for optimizing the SIR threshold in maximizing the network outage rate. Moreover, a closed-form expression is provided to estimate the number of users in the f-FAMA network in which the outage rate begins to plateau. Numerical results show that the proposed SIR threshold achieves near-maximal outage rate performance.

1 | INTRODUCTION

1.1 | Context

Enhanced mobile broadband (eMBB), ultra-reliable and low-latency communication (URLLC) and massive machine-type communication (mMTC) are the three main use cases for 5G. They are anticipated to be even more demanding in 6G and provide the context for the development of future mobile technologies [1]. Over the past decades, multiple-input multiple-output (MIMO) was the leading effort that provided the upgrades for mobile communications, with its latest edition being massive MIMO with 64 base station (BS) antennas [2]. Recent research also turned the attention to deploying large reconfigurable intelligent surfaces (RISs) [3–5] that can help optimize the radio environment for improved coverage. RIS and MIMO, however, are system-based solutions that involve both hardware and software updates that need standardization activities to realize. There is also the idea of non-orthogonal multiple access (NOMA) [6–9] which proposes to enhance the network capacity or connectivity by overlapping users on the same radio channel but will require the use of successive interference cancellation (SIC) for multiuser detection at each user. Despite the interest, NOMA has been largely limited to two-user cases due to decoding delay and complexity.

Finding a better multiple access technology that can deliver eMBB, URLLC and mMTC has been the aspiration for many researchers. Technologies such as MIMO, RIS, NOMA etc., despite their impressive performance, do impose considerable complexity in channel estimation, coordination and optimization, as well as resource allocation. A more scalable, flexible and upgradable solution is preferred. An emerging technology which may fit the bill, is fluid antenna system [10, 11].

1.2 | Fluid antenna and its application to multiple access

Fluid antenna is a radical antenna technology that represents any software-controllable, fluidic, conductive or dielectric radiating structure that can modify on demand their shape and/or position to reconfigure the operating frequency, radiation

pattern and other characteristics. In other words, the fluid antenna concept liberates antenna from the rigid radiation properties in conventional solid, metallic antennas. They can be realized by liquid-based radiating structures [12, 13] or reconfigurable pixels [14–16]. Recent efforts tended to focus on the former whereas the latter might offer delay-free reconfigurability in antenna. It is also worth mentioning two famous examples of fluid antenna. The first was the Mitsubishi Electric's seawater antenna that shot a seawater plume with a radiation efficiency of 70% [17]. Another high-profile success appeared to be the advanced saltwater-based beam-steering system developed by Nanjing University of Aeronautics and Astronautics [18, 19]. Recent researches have shown encouraging results suggesting feasibility of the concept and led to several reconfigurable fluid antenna designs, for example, [20–25]. The article [26] even provides a survey and discusses the prospect of having a fluid antenna array (i.e. fluid MIMO) at BS and/or mobile devices.

Among the various reconfigurability enabled by fluid antennas, one novel idea is to change the position of the antenna (referred to as 'port') for maximizing the signal-to-noise ratio (SNR) or the signal-to-interference ratio (SIR) in the multiuser case. This provides a novel way of obtaining spatial diversity in a small space of user equipment (UE). In [27–29], Wong et al. investigated such scenarios for single-user, point-to-point communication systems where the receiver adopts a position-switchable fluid antenna. The results illustrated that even with a small space, enormous diversity could be obtained to reduce the outage probability if the resolution of fluid antenna is large. Besides, the diversity gain can be translated into a significant capacity gain [29]. Recent research also studied fluid antenna systems in Nakagami channels [30], their diversity order [31] and level crossing rates [32]. Recently in [33], Khammassi et al. employed a fully correlated channel model that accurately characterizes the channel correlation between any two ports in a fluid antenna and reported that the system performance is affected more by the size of the antenna than the resolution. Channel estimation for fluid antenna systems was investigated in [34]. Recently, movable antenna systems, a subbranch of fluid antenna systems, have also emerged for the single-input single-output (SISO) [35] and MIMO cases [36].

While most efforts in fluid antenna communication systems are limited to single-user scenarios, for example, [27–36], the fact that a position-switchable fluid antenna can access the ups and downs of fading envelope of the interference can be exploited for multiple access. Specifically, a fluid antenna assisted UE is gifted with the ability to tune in to the window of opportunity in which the interference naturally disappears in a deep fade, without prior coordination nor advanced signal processing, all by a single radio frequency (RF)-chain fluid antenna switching its port to the most desirable one. This approach is referred to as fluid antenna multiple access (FAMA) [10].

There are two types of FAMA: (i) fast FAMA (f-FAMA) [37–39] and (ii) slow FAMA (s-FAMA) [40]. For s-FAMA, the fluid antenna of each user selects the port that maximizes the average received signal-to-interference plus noise ratio (SINR) in which the averaging is taken over the transmitted data of all the users. In this case, the fluid antenna looks for the point in space where the channel envelopes of all the interferers fade deeply simultaneously. The effectiveness of this approach depends on the likelihood of deep fades of each interferer's channel envelope. On the other hand, the rationale of f-FAMA is different and that the fluid antenna seeks the port where the ratio between the desired user's channel gain to the energy of the *instantaneous* sum-interference plus noise signal is maximized. In this approach, the ratio depends on how the instantaneous data-bearing interference signals (and noise) combine. A key difference is that s-FAMA requires the fluid antenna to switch only when the channels change but f-FAMA needs the fluid antenna to switch at every symbol instance. In terms of network capacity performance, s-FAMA can support a few users whereas f-FAMA easily can handle tens or hundreds of users. Clearly, fluid antenna systems can contribute to eMBB and mMTC. Their application to URLLC was discussed in [10] which also provided an overall view of the roles of fluid antenna in mobile communications.

1.3 | Novelty and contributions

In this paper, we investigate a downlink channel in which a multi-antenna BS is communicating to U UEs, each equipped with a fluid antenna of size $W\lambda$ and N ports[1] where λ denotes the wavelength. In particular, each BS antenna is dedicated to transmitting information to one specific UE. In other words, no beamforming is adopted at the BS and the BS needs only U antennas. At each UE, same as in [37], f-FAMA is considered, meaning that the UE always switches to the port maximizing the signal energy to sum-interference energy ratio.[2] We assume that the BS is transmitting a common fixed coding rate to each UE, specified by an SIR threshold γ. In this case, we have the average network outage rate given by [37, (21)]

$$C(\gamma) = U(1 - p_{\text{out}}(\gamma))\log_2(1+\gamma), \tag{1}$$

where $p_{\text{out}}(\gamma)$ denotes the outage probability at each UE. This capacity definition follows from the result in [41] when the transmitter transmits a fixed coding rate.[3]

Despite the results in [37–40], FAMA research is still in an early stage. In particular, the SIR threshold, γ, is always fixed and arbitrarily given. Nonetheless, as seen in (1), the network rate is a function of γ. If γ is very small, then the rate for each UE will

[1] Note that N can be a large number. Liquid-based fluid antennas can be mobilized almost anywhere within a predefined space. Even for reconfigurable pixel-based fluid antennas [14–16], a standard mobile handset has dimensions of $160.8 \times 78.1 \times 7.7$mm, with a display resolution of up to 1284×2778 pixels. Therefore, it is reasonable to contemplate a fluid antenna to have, say $N = 1500$ ports (or RF pixels) on a handset in the future.

[2] It is worth pointing out that f-FAMA needs port switching on a symbol by symbol basis. Thus, the fluid antenna should be based on the reconfigurable pixel antenna designs (e.g. [14–16]) to perform delay-free switching. On the other hand, for conciseness, we will abuse the notation and regard the ratio between the instantaneous signal energy to the energy of the sum-interference plus noise as SIR. Estimating this ratio over all the ports at a symbol by symbol basis is indeed challenging but it has been addressed in [39]. In this paper, we will assume that perfect estimation is always achieved and our focus will be on the performance of f-FAMA with perfect port selection.

[3] In (1), the UEs are assumed statistically identical for ease of discussion. Mathematically, the analysis is not more difficult but tedious if they are not.

be low and so does the network rate. On the other hand, if γ is too large, $p_{\text{out}}(\gamma) \to 1$ and the network rate will be very low as well. Therefore, there should be an optimal γ such that $C(\gamma)$ peaks. This phenomenon has been illustrated in [37, Fig. 4]. As a matter of fact, $C(\gamma)$ also depends on the number of users, U, as more users will increase connectivity but at the expense of compromising $p_{\text{out}}(\gamma)$. Motivated by this, our aim is to study the maximization of $C(\gamma)$.

Technically speaking, we achieve this by deriving an approximation of the outage probability $p_{\text{out}}(\gamma)$ in closed form so that a closed-form expression for $C(\gamma)$ is available for maximization. As a consequence, several important results including a closed-form approximation for the optimal γ can be obtained. In addition, we will show that $C(\gamma)$ is in fact a monotonic increasing function of U if γ is optimized. However, theoretically, as $U \to \infty, \gamma \to 0$, thereby compromising the individual rate performance. As a result, we propose to strike the balance of $C(\gamma)$ and γ by estimating the number of users, U, where the network rate begins to plateau.

Before proceeding to the main body of this paper, we here state some of our principal results. This summary aims to give the reader an overall view of the material covered in this paper and highlight our main contributions.

- For $W \geq 1$, the outage probability for a UE, with an SIR target γ, can be approximated as

$$p_{\text{out}}(\gamma) \approx \left[1 - \frac{N\left(1 - \frac{1}{\pi W}\right)}{(U-1)\gamma}\right]^{+},$$

  where $(a)^{+} = \max\{0, a\}$. This result illustrates how the interference immunity depends on the parameters N, γ, U and W. A clear distinction of the performance between f-FAMA and s-FAMA can be observed by comparing the above approximate expression and the result in [40].
- For a given SIR threshold, γ, the terminal network rate, as $U \to \infty$, can be approximated as

$$\lim_{U\to\infty} C(\gamma) \approx \left[\frac{N\left(1 - \frac{1}{\pi W}\right)}{\gamma} + 1\right] \log_2(1+\gamma).$$

- For a given SIR threshold, γ, $C(\gamma)$ begins to plateau if U is increased to

$$U^{*} = \frac{N\left(1 - \frac{1}{\pi W}\right)}{\gamma} + 1.$$

- For a given U, the optimal SIR threshold, γ^{*}, maximizing the network rate, $C(\gamma)$, can be approximated by

$$\gamma^{*} \approx \frac{N\left(1 - \frac{1}{\pi W}\right)}{U-1}.$$

- With UEs each with size of $W\lambda$ and N ports, and that an optimal SIR threshold, γ^{*}, is selected, as $U \to \infty$, the maximum network outage rate limit is found as

$$\lim_{U\to\infty} C(\gamma^{*}) = (1-\rho)\frac{N\left(1 - \frac{1}{\pi W}\right)}{\ln 2} \quad \text{(in bps/channel use)},$$

  where $1-\rho$ is a discount factor and ρ denotes the outage probability which depends only on W and N.

The rest of the paper is organized as follows. In Section 2, we introduce the system model of f-FAMA in the downlink. Section 3 then presents the analytical results that are useful in the maximization of $C(\gamma)$ which will be addressed in Section 4. Section 5 provides the numerical results that corroborate the analysis. Finally, Section 6 concludes this paper.

2 | SYSTEM MODEL FOR f-FAMA

We consider a downlink system where there are U UEs and the BS uses one of its antennas to transmit information to one specific UE. Each of the BS antenna is assigned to handle one particular UE. The BS antennas are assumed to be located far enough so that their channels to a given UE are independent. Each UE adopts an N-port fluid antenna of size $W\lambda$, meaning that there are N positions evenly distributed over $W\lambda$ that the radiating element of fluid antenna can be switched to. As such, we can write the received signal at the k-th port of UE u as

$$r_k^{(u)} = s_u g_k^{(u,u)} + \underbrace{\sum_{\tilde{u}=1, \tilde{u}\neq u}^{U} s_{\tilde{u}} g_k^{(\tilde{u},u)}}_{\tilde{g}_k^{(u)}} + \eta_k^{(u)}, \tag{2}$$

where s_u denotes the transmitted symbol for UE u, $\eta_k^{(u)}$ is the zero-mean complex additive white Gaussian noise (AWGN) at the k-th port for UE u, $g_k^{(\tilde{u},u)}$ denotes the fading channel from the BS' $\tilde{u}$-th antenna to the k-th port of UE u, and $\tilde{g}_k^{(u)}$ denotes the sum-interference signal at a symbol instant.

The fluid antenna at UE u is assumed to instantly switch to the best port, k_u^{*}, for maximizing the energy of the designed signal to the energy of the sum-interference ratio, or SIR at the symbol level.[4] Consequently, we have

$$k_u^{*} = \arg\max_k \text{SIR}_k \equiv \arg\max_k \frac{\left|g_k^{(u,u)}\right|^2}{\left|\tilde{g}_k^{(u)}\right|^2}. \tag{3}$$

[4] In this paper, any switching delay is assumed negligible. In practice, port switching may be done instantly seemingly without delay if reconfigurable pixel-based fluid antennas [14–16] are considered.

Note that how to estimate the port SIR at each symbol itself has been addressed in [39]. Some ideas on this have also been discussed in [10]. In this paper, we assume that (3) is always achieved for communications to all the UEs.

We model the amplitude of the channel, $|g_k^{(\tilde{u},u)}|$, as Rayleigh distributed random variable, with the probability density function (pdf) given by[5]

$$p_{|g_k^{(\tilde{u},u)}|}(r) = re^{-\frac{r^2}{\sigma^2}}, \text{ for } r \geq 0 \text{ with } \mathrm{E}[|g_k^{(\tilde{u},u)}|^2] = \sigma^2. \quad (4)$$

The average received SNR at each port is given by $\Gamma = \frac{\sigma^2\sigma_s^2}{\sigma_\eta^2}$ where $\sigma_s^2 = \mathrm{E}[|s_u|^2]$ and σ_η^2 is the noise power. The channels $\{g_k^{(\tilde{u},u)}\}_{\forall k}$ are considered to be correlated as they can be arbitrarily close to each other. To model the correlation between the channels at the ports, we parameterize $g_k^{(\tilde{u},u)}$, through a single correlation parameter μ, as [38]

$$\begin{aligned} g_k^{(\tilde{u},u)} &= \sigma\left(\sqrt{1-\mu^2}x_k^{(\tilde{u},u)} + \mu x_0^{(\tilde{u},u)}\right) \\ &\quad + j\sigma\left(\sqrt{1-\mu^2}y_k^{(\tilde{u},u)} + \mu y_0^{(\tilde{u},u)}\right), \\ k &= 1, 2, \ldots, N, \end{aligned} \quad (5)$$

where $x_0^{(\tilde{u},u)}, \ldots, x_N^{(\tilde{u},u)}, y_0^{(\tilde{u},u)}, \ldots, y_N^{(\tilde{u},u)}$ are all independent zero-mean Gaussian random variables with variance of 0.5. Note that the correlation among the ports is introduced through the common random variables $x_0^{(\tilde{u},u)}$ and $y_0^{(\tilde{u},u)}$. Also,

$$\mu = \sqrt{2}\sqrt{{}_1F_2\left(\frac{1}{2}; 1, \frac{3}{2}; -\pi^2W^2\right) - \frac{J_1(2\pi W)}{2\pi W}}, \quad (6a)$$

$$\approx \begin{cases} 1 - \dfrac{\pi^2W^2}{12}, & \text{for } W \leq 0.6, \\ \dfrac{1}{\sqrt{\pi W}}, & \text{for } W \geq 1, \end{cases} \quad (6b)$$

where ${}_aF_b(\cdot;\cdot;\cdot)$ denotes the generalized hypergeometric function and $J_1(\cdot)$ is the first-order Bessel function of the first kind. The condition (6) ensures the fluid antenna to have the same mean correlation coefficient for an N-port linear structure of length $W\lambda$ [38, Theorem 1] and the approximation is due to [38, Theorem 2], which will be useful to link the achievable performance of f-FAMA to the size of fluid antenna. Due to (6b), we will regard '$W \leq 0.6$' as *small* W and '$W \geq 1$' as *large* W. Additionally, given this channel model (5), it is rather easy to extend it to the two-dimensional (2D) case. The only thing that needs to be adjusted is the choice of the correlation parameter, μ, which needs to be derived again based on a 2D structure. This was briefly discussed in [10].

Our channel correlation model (5) is based on the generalized channel correlation model by Beaulieu et al. in [44], with the correlation parameters set according to [38, Theorem 1]. Evidently, there are other models. One emerging model, popularly used for the millimeter-wave band, is the multi-ray channel model [45, 46]. This model is particularly attractive because it is possible to select detailed channel parameters to represent specific fading phenomena, but the major drawback is that it loses the mathematical tractability that the generalized channel correlation model in [44] possesses. Fortunately, it was shown in [40] that the results obtained from the model in [38] and that in [45, 46] are similar if the SIR threshold, γ, is not too large. As a result, with the much improved tractability, we have preferred to adopt the generalized channel correlation model in [38]. We also note that [33] recently employed an accurate channel model in characterizing the spatial correlation among the ports but its tractability is very limited.

The primary performance metric of the f-FAMA network is the outage probability for a typical UE, that is

$$p_{\text{out}}(\gamma) = \text{Prob}\left(\text{SIR} = \max_k \text{SIR}_k < \gamma\right), \quad (7)$$

for a given SIR threshold, γ. Note that here, a typical UE is considered and therefore the user index, u, is omitted. Without loss of generality, we assume $\sigma_s^2 = 1$ and according to [37, Theorem 1] and [38, (17)], the outage probability (7) can be expressed as

$$\begin{aligned} p_{\text{out}}(\gamma) = \int_0^\infty e^{-z}\int_0^\infty e^{-t}\Bigg[1 + \left(\frac{a^2}{a^2+1}\right)e^{-\left(\frac{1}{a^2+1}\right)\frac{\mu^2}{1-\mu^2}\left(a^2z+t\right)} \\ \times I_0\left(\frac{a}{a^2+1}\left(\frac{2\mu^2}{1-\mu^2}\right)\sqrt{zt}\right) \\ - Q_1\left(\frac{1}{\sqrt{a^2+1}}\sqrt{\frac{2\mu^2}{1-\mu^2}}\sqrt{t}, \frac{a}{\sqrt{a^2+1}}\sqrt{\frac{2\mu^2}{1-\mu^2}}\sqrt{z}\right)\Bigg]^N dtdz, \end{aligned} \quad (8)$$

in which $I_0(\cdot)$ is the zero-order modified Bessel function of the first kind, $Q_1(\cdot,\cdot)$ is the first-order Marcum Q-function, and $a = \sqrt{(U-1)\gamma}$.

3 | OUTAGE PROBABILITY ANALYSIS

This section presents a closed-form approximation to (8) which will enable the maximization of $C(\gamma)$ in (1). Before we present the main result, the following lemmas are useful.

Lemma 1.

$$\int_0^\infty e^{-\alpha t}I_0(\beta\sqrt{t})dt = \frac{1}{\alpha}e^{\frac{\beta^2}{4\alpha}}, \text{ for } \alpha, \beta > 0. \quad (9)$$

[5] In a rich scattering environment, the most accurate statistical model for the wireless channel is the Rayleigh fading model [42]. This comes naturally from the fact that a large number of paths with random amplitudes and phase shifts will superimpose to produce a resultant channel coefficient with a Rayleigh distributed amplitude and a uniformly distributed phase shift as a consequence of central limit theorem. The Rayleigh statistical channel model has also been validated by numerous experiments [43].

Proof. Using [47, (B.31)] by setting $b = 0$ and $c = \beta$, we obtain

$$\int_0^\infty x e^{-\frac{p^2x^2}{2}} I_0(\beta x)dx = \frac{1}{p^2} e^{\frac{\beta^2}{2p^2}}. \tag{10}$$

Now, changing the variable by $x^2 = t$ and also setting $\alpha = \frac{p^2}{2}$, we get the desired result (9), which completes the proof. □

Lemma 2.

$$\int_0^\infty e^{-t} Q_1(\alpha\sqrt{t}, \beta)dt = Q_1\left(0, \frac{\sqrt{2}\beta}{\sqrt{\alpha^2+2}}\right). \tag{11}$$

Proof. Using [47, (B.31)] by setting $c = 0$, $a = \alpha$ and $b = \beta$, we get

$$\int_0^\infty x e^{-\frac{p^2x^2}{2}} Q_1(\alpha x, \beta)dx = \frac{1}{p^2} Q_1\left(0, \frac{\beta p}{\sqrt{\alpha^2+p^2}}\right). \tag{12}$$

Changing the variable by $x^2 = t$ and also setting $p = \sqrt{2}$, we get the desired result (11), which completes the proof. □

Lemma 3.

$$\int_0^\infty e^{-t} Q_1(0, \alpha\sqrt{t})dt = \frac{2}{\alpha^2+2}. \tag{13}$$

Proof. Using [47, (B.32)] by setting $a = \alpha$, $b = 0$, $c = 0$ and $p = \sqrt{2}$, we have

$$\begin{aligned}\int_0^\infty x e^{-x^2} Q_1(0, \alpha x)dx &= \frac{1}{2}\left[Q_1(0,0) - \frac{\alpha^2}{\alpha^2+2}\right] \\ &= \frac{1}{2}\left[1 - \frac{\alpha^2}{\alpha^2+2}\right] = \frac{1}{\alpha^2+2}.\end{aligned} \tag{14}$$

Finally, changing the variable by $x^2 = t$ gives (13). □

Theorem 1. *The outage probability for a typical f-FAMA user with an SIR threshold, γ, can be approximated as*

$$p_{\text{out}}(\gamma) \approx \left[1 - \frac{N(1-\mu^2)}{a^2+1} - \frac{N\mu^2}{a^2+1}\right]^+. \tag{15}$$

Substituting $a^2 = (U-1)\gamma$ and for large U, we can write

$$p_{\text{out}}(\gamma) \approx \begin{cases} \left[1 - \dfrac{N\left(1 - \frac{1}{\pi W}\right)}{(U-1)\gamma}\right]^+, \textit{for large} W, \\ \left[1 - \dfrac{N\left(1 - \frac{\pi^2 W^2}{6}\right)}{(U-1)\gamma}\right]^+, \textit{for small} W. \end{cases} \tag{16}$$

Proof. See Appendix A. □

Corollary 1. *In the linear region in which the multiplexing gain, m, is a linear function of N, the multiplexing gain for the f-FAMA network can be approximated as*

$$m \approx \begin{cases} \dfrac{N\left(1 - \frac{1}{\pi W}\right)}{\gamma}, \textit{for large} W, \\ \dfrac{N\left(1 - \frac{\pi^2 W^2}{6}\right)}{\gamma}, \textit{for small} W. \end{cases} \tag{17}$$

Proof. Using the definition of multiplexing gain, we have

$$m = U(1 - p_{\text{out}}(\gamma)). \tag{18}$$

Now, using the approximations (16) and ignoring the sign $[\cdot]^+$ in the linear region to express $p_{\text{out}}(\gamma)$ in (18), the result (17) is obtained, which completes the proof. □

The expression for large W in (17) coincides with [37, (28)] which was otherwise obtained through an upper bound. Note that the result for small W in (17) looks different from that in [38, (12)]. This is due to the fact that the result in [38, (12)] came from an outage probability upper bound which was only valid for large W but then the new result in (17) was obtained from (15) which is valid for any value of W.

Lastly, it should be noted that Corollary 1 is only applicable for the linear region of m and $m \leq U$ is always true.

4 | NETWORK RATE MAXIMIZATION

In this section, we develop the analytical results that maximize the network outage rate, $C(\gamma)$, given by (1), that is

$$\bar{C} = \max_{\gamma} C(\gamma) = C(\gamma^*). \tag{19}$$

The motivation is that the network outage rate depends on the SIR threshold γ which should be optimized. Our results focus on the large W case (i.e. $W \geq 1$) as W should not be too small to have enough opportunity for interference null for a meaningful performance in multiple access.

Theorem 2. *For a given number of users, U, $C(\gamma)$ can be maximized by choosing the SIR threshold as*

$$\gamma^* = \frac{N\left(1-\frac{1}{\pi W}\right)}{U-1}, \tag{20}$$

which gives

$$\bar{C} = U\log_2\left[1+\frac{N\left(1-\frac{1}{\pi W}\right)}{U-1}\right]. \tag{21}$$

Proof. Applying (16) on (1), we can obtain

$$C(\gamma) = \begin{cases} \frac{UN\left(1-\frac{1}{\pi W}\right)}{(U-1)\gamma}\log_2(1+\gamma) & \text{if } \gamma > \frac{N\left(1-\frac{1}{\pi W}\right)}{U-1}, \\ U\log_2(1+\gamma) & \text{otherwise.} \end{cases} \tag{22}$$

Taking the derivative of $C(\gamma)$ with respect to (w.r.t.) γ gives

$$\frac{\partial C(\gamma)}{\partial \gamma} = \begin{cases} C_1'(\gamma) \text{ if } \gamma > \frac{N\left(1-\frac{1}{\pi W}\right)}{U-1}, \\ \frac{U}{(\ln 2)(1+\gamma)} \text{ otherwise,} \end{cases} \tag{23}$$

where

$$C_1'(\gamma) = \frac{U(1-p_{\text{out}}(\gamma))}{(\ln 2)(1+\gamma)} - \frac{U\ln(1+\gamma)}{\ln 2}\left(\frac{\partial p_{\text{out}}(\gamma)}{\partial \gamma}\right), \tag{24}$$

in which

$$\frac{\partial p_{\text{out}}(\gamma)}{\partial \gamma} = \frac{N\left(1-\frac{1}{\pi W}\right)}{(U-1)\gamma^2}. \tag{25}$$

Substituting (25) and (16) into (24), we can write

$$C_1'(\gamma) = \frac{UN\left(1-\frac{1}{\pi W}\right)}{(\ln 2)(U-1)\gamma}\left[\frac{1}{1+\gamma} - \frac{\ln(1+\gamma)}{\gamma}\right] < 0. \tag{26}$$

Hence, if $\gamma > \frac{N(1-\frac{1}{\pi W})}{U-1}$, $C_1'(\gamma) < 0$. Also, note in (23) that if $\gamma \leq \frac{N(1-\frac{1}{\pi W})}{U-1}$, $\frac{\partial C(\gamma)}{\partial \gamma} = \frac{U}{(\ln 2)(1+\gamma)} > 0$. As a result, the maximum of $C(\gamma)$ occurs at (20). Finally, substituting (20) into (1) gives (21), which completes the proof. □

The next theorem characterizes the property of $C(\gamma)$ for a given SIR threshold γ when the number of users, U, increases.

Theorem 3. *With an SIR threshold, γ, the average network outage rate, $C(\gamma)$, is an increasing function of the number of users, U, and $C(\gamma)$ begins to plateau if U reaches*

$$U^* = \frac{N\left(1-\frac{1}{\pi W}\right)}{\gamma} + 1, \tag{27}$$

at which the network outage rate becomes

$$C(\gamma) = \left[\frac{N\left(1-\frac{1}{\pi W}\right)}{\gamma} + 1\right]\log_2(1+\gamma). \tag{28}$$

Proof. Using the rate expression (22) and rearranging the condition with U as the subject, we get

$$C(\gamma) = \begin{cases} \frac{UN\left(1-\frac{1}{\pi W}\right)}{(U-1)\gamma}\log_2(1+\gamma) & \text{if } U > \frac{N\left(1-\frac{1}{\pi W}\right)}{\gamma} + 1, \\ U\log_2(1+\gamma) & \text{otherwise.} \end{cases} \tag{29}$$

Now, taking the derivative of the above, we then have

$$\frac{\partial C(\gamma)}{\partial U} = \begin{cases} C_2'(\gamma) & \text{if } U > \frac{N\left(1-\frac{1}{\pi W}\right)}{\gamma} + 1, \\ \log_2(1+\gamma) & \text{otherwise,} \end{cases} \tag{30}$$

where

$$C_2'(\gamma) = -\frac{N\left(1-\frac{1}{\pi W}\right)}{\gamma}\frac{\log_2(1+\gamma)}{(U-1)^2} \approx 0, \text{ for large} U. \tag{31}$$

In summary, if $U < \frac{N(1-\frac{1}{\pi W})}{\gamma} + 1$, then $C(\gamma)$ will continue to increase as U increases but plateau when $U > \frac{N(1-\frac{1}{\pi W})}{\gamma} + 1$. Substituting (27) into (29) obtains (28). □

Theorem 3 suggests that one should increase the network rate by packing more users onto the same radio resource unit using f-FAMA. However, according to Theorem 2, the optimal SIR threshold is inversely proportional to $U-1$, see (20). As a result, the maximization of $C(\gamma)$ comes with a compromise on the individual's rate performance. In the extreme case where $U \to \infty$, $\gamma^* \to 0$. For this reason, it would make more sense to set the SIR threshold, γ, based on the required performance at each UE and then operate the network with the number of users by (27), approaching the network's maximum rate.

The following theorem considers the case where the SIR threshold γ is always optimized and examines the maximum rate limit if the number of users, U, grows without bound.

Theorem 4. *Given the number of ports, N, and size W for the fluid antenna at each UE and that the optimal SIR threshold (20) is selected,*

the maximum network rate approaches

$$C(\gamma^*) \to (1-\rho)\frac{N(1-\mu^2)}{\ln 2}, \text{ as } U \to \infty, \tag{32}$$

where $\rho = p_{\text{out}}$*, after substituting* $a = \sqrt{N(1-\mu^2)}$ *in (8), depends only on* W *and* N*, and* μ *can be obtained by (6).*

Proof. First, we take the capacity expression (1) and then substitute $\gamma = \gamma^*$ in (20) to obtain

$$a = \sqrt{(U-1)\gamma^*} = \sqrt{(U-1)\frac{N(1-\mu^2)}{(U-1)}} = \sqrt{N(1-\mu^2)}. \tag{33}$$

As a result, we have $p_{\text{out}} = \rho$ in (1).

Now, we take the limit $U \to \infty$ of the resulting network rate expression (1), which gives

$$\begin{aligned}
&\lim_{U\to\infty} C(\gamma^*) \\
&= \lim_{U\to\infty} U(1-\rho)\log_2\left[1+\frac{N(1-\mu^2)}{U-1}\right] \\
&= \lim_{U\to\infty} (1-\rho)\frac{\log_2\left[1+\frac{N(1-\mu^2)}{U-1}\right]}{\left(\frac{1}{U}\right)} \\
&\overset{(a)}{=} \lim_{U\to\infty} (1-\rho)\frac{\left(\frac{1}{\ln 2}\right)\frac{N(1-\mu^2)}{\left[1+\frac{N(1-\mu^2)}{U-1}\right]}\left(-\frac{1}{(U-1)^2}\right)}{\left(-\frac{1}{U^2}\right)} \\
&= (1-\rho)\frac{N(1-\mu^2)}{\ln 2},
\end{aligned} \tag{34}$$

where (*a*) uses L'Hôpital's rule to evaluate the limit. □

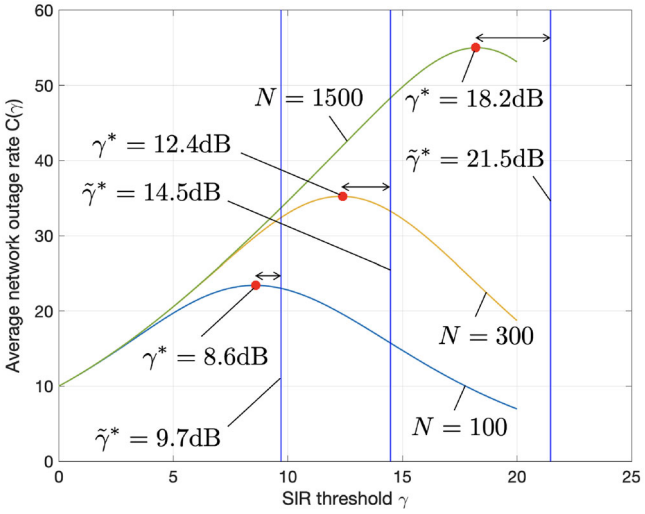

FIGURE 1 The average network outage rate for f-FAMA systems against the SIR threshold, γ, when $W = 2$ and $U = 10$.

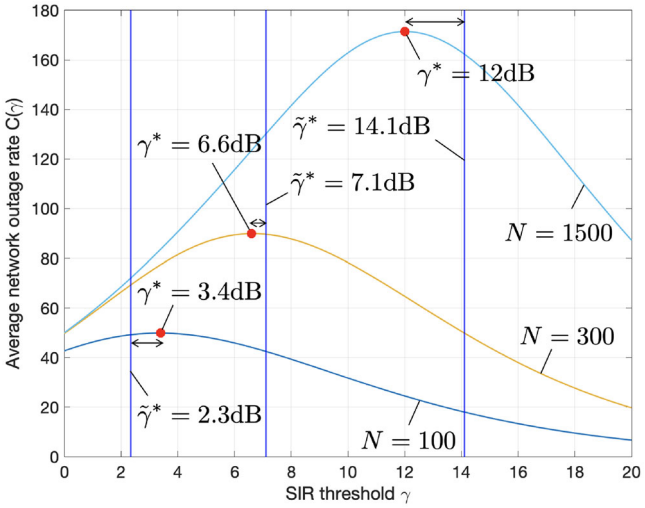

FIGURE 2 The average network outage rate for f-FAMA systems against the SIR threshold, γ, when $W = 2$ and $U = 50$.

5 | NUMERICAL RESULTS AND DISCUSSION

In this section, we provide numerical results to verify our analysis and gain insight into the performance of f-FAMA. To help with the discussion, it is assumed that all the UEs and their channels are statistically identical and also that noise is ignored. The results in Figures 1–3 are provided for the network outage rates against the SIR threshold for $U = 10, 50, 100$, respectively. All the results considered $W = 2$ (i.e., the fluid antenna at each UE has the size of 2λ). This is motivated by the fact that if the carrier frequency is $f = 5$GHz, then the wavelength is $\lambda = 6$ cm and a dimension of 12 cm (a typical size of a mobile device) will have $W = 2$.

In each of the figures, the results for $N = 100, 300, 1500$ are provided. The red dots represent the actual optimal SIR threshold, γ^*, while the blue vertical lines show the optimal SIR threshold, $\tilde{\gamma}^*$ predicted by our analysis in (20). Several observations can be made. First of all, the results illustrate that as N increases, γ^* increases accordingly. This makes sense because a high-resolution fluid antenna at each UE should allow a stronger SIR threshold to be fulfilled. Additionally, the predicted optimal SIR threshold is generally very close to the actual optimum. Although the distance between γ and $\tilde{\gamma}^*$ gets slightly larger if N is larger, the degradation in the network rate is small, $C(\gamma^*) \approx C(\tilde{\gamma}^*)$. Furthermore, the results show that if U increases, the optimal SIR threshold, γ^*, decreases, as expected. Overall, $\tilde{\gamma}^*$ remains very accurate.

Figure 4 investigates the impact of W on the accuracy of the predicted SIR threshold, $\tilde{\gamma}^*$, when $U = 50$ and $N = 100$. The values $W = 0.5, 1, 2$ are considered, which, respectively, correspond to $f = 1.25, 2.5, 5$ GHz with a size of $W\lambda = 12$ cm fluid antenna. As can be seen, if W is larger, then the network rate $C(\gamma)$ increases as expected. However, there is a

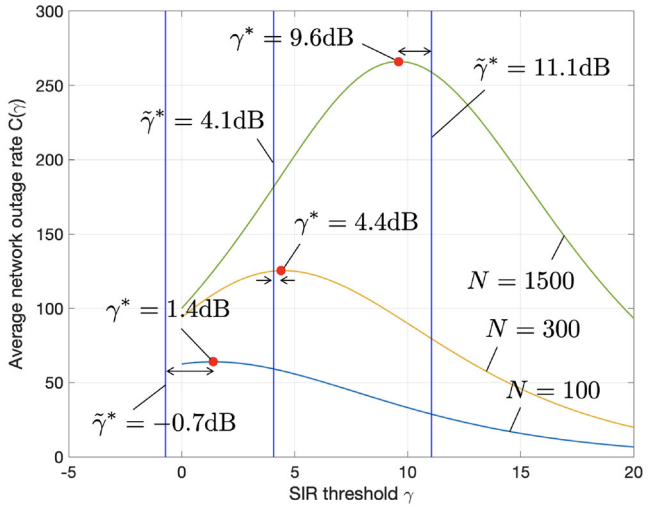

FIGURE 3 The average network outage rate for f-FAMA systems against the SIR threshold, γ, when $W = 2$ and $U = 100$.

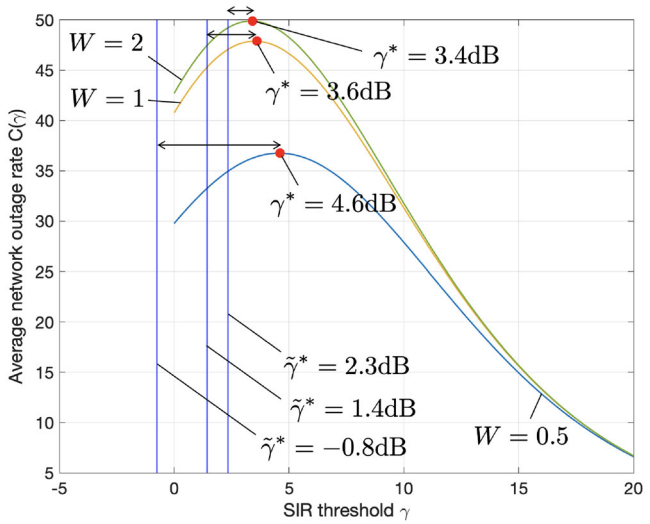

FIGURE 4 The average network outage rate for f-FAMA systems against the SIR threshold, γ, when $N = 100$ and $U = 50$.

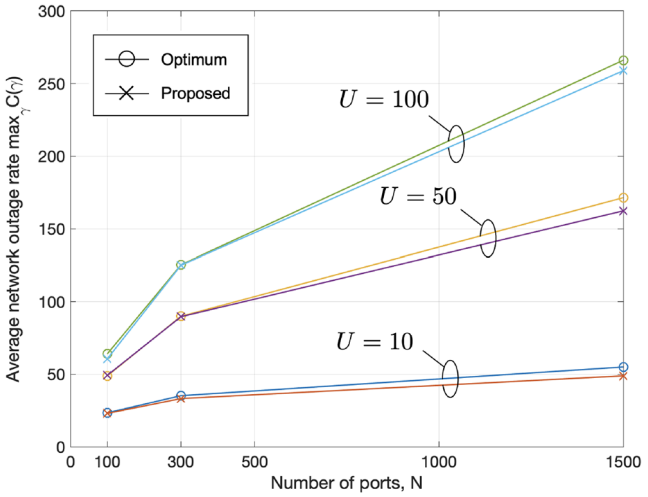

FIGURE 5 The average network outage rates for f-FAMA systems against the number of ports, N, using γ^* and $\tilde{\gamma}^*$ when $W = 2$.

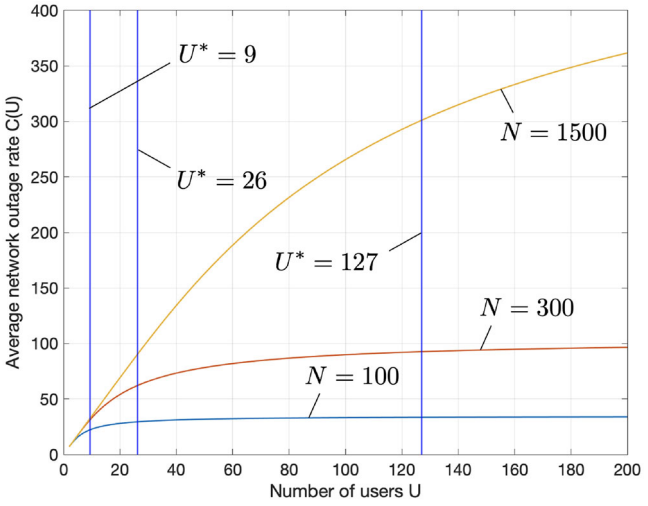

FIGURE 6 The average network outage rate for f-FAMA systems against the number of users, U, when $\gamma = 10$ and $W = 2$.

diminishing return in the capacity gain which was also reported in [37]. Besides, the optimal SIR threshold, γ^*, decreases only very slightly as W increases. For small W, the distance between γ^* and $\tilde{\gamma}^*$ is obviously larger while the prediction by $\tilde{\gamma}^*$ is very good for large W. Despite this, the network outage rate $C(\tilde{\gamma}^*)$ is very close to the maximum $C(\gamma^*)$ regardless of the value of W. This comparison is facilitated by the results in Figure 5 in which the optimal one refers to the use of the optimal SIR threshold γ^* in obtaining the network rate $C(\gamma^*)$ and the proposed one uses $\tilde{\gamma}^*$ in (20). The results reveal that the proposed system obtains a near maximum network rate for the entire range of N although the accuracy seems to improve when the value of N gets smaller.

Now, we use the results in Figure 6 to investigate how the network rate scales with the number of users, U, when $W = 2$ and the SIR threshold is fixed at $\gamma = 10$. As expected, the results show that the network rate increases with both N and U. In the figure, we also provide several vertical lines marking the number of users U^* estimated by (27) which predict the number of users at which the network rate should begin to plateau. The results suggest that (27) appears to be a very good estimate. In addition, according to the network rate expression (28), we can find that the network rates are 32.5, 90.7 and 439.8 for the cases of $N = 100$, 300 and 1500, respectively. This indicates that (28) indeed gives a very good estimate for the maximum achievable network rate for given N and γ if the number of users increases without bound. This can be explained by recognizing the fact that our analysis is originated from a first-order approximation for the network outage rate. Therefore, (28) is more an estimate for the terminal network rate when $U \to \infty$ rather than the network rate at $U = U^*$.

We conclude this section by presenting the results in Figure 7 which show the maximum network rate $C(\gamma^*)$ when the SIR

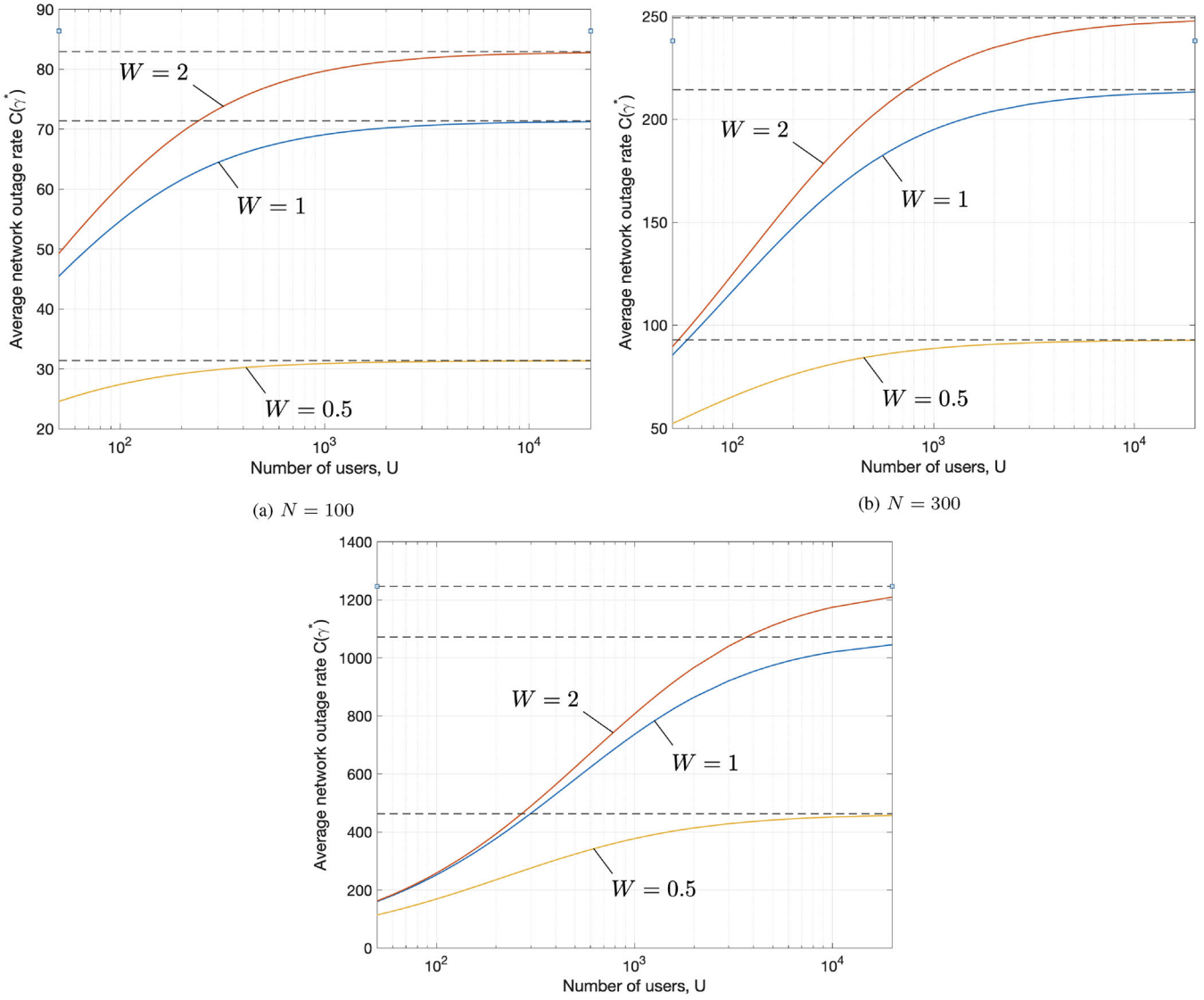

FIGURE 7 The maximum network rate against the theoretical limit (32).

threshold is always optimized, against the number of users, U. First, we see that if N increases, the network rate improves. Also, the network rate increases with the size of fluid antenna, W. In addition, the network rate has a much bigger jump from $W = 0.5$ to $W = 1$ than from $W = 1$ to $W = 2$. On the other hand, the dash lines in the figures show the network rate limits predicted by (32) when W and N are fixed. The results demonstrate that the analytical result (32) precisely estimates the network rate limit for all the cases although the number of users needs to be extremely large in order to meet the limit. It should be noted that theoretically the maximum network rate limit can be approached by using the SIR threshold (20) and having a very large number of users in the f-FAMA network. Nevertheless, with a very large U, each UE in fact has a very miserable SIR threshold (note that $\gamma^* \to 0$ as $U \to \infty$). As a consequence, it may be more reasonable to set the SIR threshold based on the required quality of service (QoS) for the UEs and then operate the f-FAMA network using the number of users according to (27), so as to strike a good balance between the network rate and individual's QoS.

6 | CONCLUSION

Understanding the fact that the network outage rate of f-FAMA depends on the SIR threshold for each UE, this paper studied the capacity maximization problem. We first derived a first-order approximation for the outage probability which was then used to conduct the maximization of the network outage rate. A closed-form expression for estimating the optimal SIR threshold was presented and we also derived the number of users where the average network outage rate began to plateau,

which provided an operating point for striking a good balance between the network rate and the individual UE's QoS. Also, we obtained the terminal network rate limit for f-FAMA when the optimal SIR threshold was used and the number of users was infinity. The numerical results verified our analysis.

AUTHOR CONTRIBUTIONS

Kai-Kit Wong: Conceptualization, formal analysis, investigation, methodology, writing - original draft. Kin Fai (Kenneth) Tong: Conceptualization, investigation, supervision, writing - review and editing. Yu Chen: Supervision, writing - review and editing. Yangyang Zhang: Supervision, writing - review and editing.

ACKNOWLEDGEMENTS

The work of K. Wong and K. Tong is supported in part by the Engineering and Physical Sciences Research Council (EPSRC) under grant EP/W026813/1. Also, the work of Y. Chen is supported by the National Natural Science Foundation of China under Grant 61901055. For the purpose of open access, the authors will apply a Creative Commons Attribution (CC BY) licence to any Author Accepted Manuscript version arising.

CONFLICT OF INTEREST STATEMENT

The authors have declared no conflict of interest.

DATA AVAILABILITY STATEMENT

Data sharing not applicable to this article as no datasets were generated or analysed during the current study.

ORCID

Kai-Kit Wong https://orcid.org/0000-0001-7521-0078
Kin-Fai Tong https://orcid.org/0000-0003-3913-0227

REFERENCES

1. Tariq, F., et al.: A speculative study on 6G. IEEE Wireless Commun. 27(4), 118–125 (2020)
2. Larsson, E.G., Edfors, O., Tufvesson, F., Marzetta, T.L.: Massive MIMO for next generation wireless systems. IEEE Commun. Mag. 52(2), 186–195 (2014)
3. Liaskos, C., et al.: A new wireless communication paradigm through software-controlled metasurfaces. IEEE Commun. Mag. 56(9), 162–169 (2018)
4. Basar, E., et al.: Wireless communications through reconfigurable intelligent surfaces. IEEE Access 7, 116753–116773 (2019)
5. Di Renzo, M., et al.: Smart radio environments empowered by reconfigurable AI meta-surfaces: An idea whose time has come. EURASIP J. Wireless Commun. Netw. 2019(129), (2019)
6. Saito, Y., Kishiyama, Y., Benjebbour, A., Nakamura, T., Li, A., Higuchi, K.: Non-orthogonal multiple access (NOMA) for cellular future radio access. In: Proceedings of IEEE 77th Vehicular Technology Society (VTC Spring), pp. 1–5. IEEE, Piscataway (2013)
7. Dai, L., Wang, B., Yuan, Y., Han, S., Chih-lin, I., Wang, Z.: Non-orthogonal multiple access for 5G: Solutions, challenges, opportunities, and future research trends. IEEE Commun. Mag. 53(9), 74–81 (2015)
8. Ding, Z., Lei, X., Karagiannidis, G.K., Schober, R., Yuan, J., Bhargava, V.K.: A survey on non-orthogonal multiple access for 5G networks: Research challenges and future trends. IEEE J. Sel. Areas Commun. 35(10), 2181–2195 (2017)
9. Ye, N., An, J., Yu, J.: Deep-learning-enhanced NOMA transceiver design for massive MTC: Challenges, state of the art, and future directions. IEEE Wireless Commun. 28(4), 66–73 (2021)
10. Wong, K.K., Tong, K.F., Shen, Y., Chen, Y., Zhang, Y.: Bruce Lee-inspired fluid antenna system: Six research topics and the potentials for 6G. Frontiers Commun. Netw., Wireless Commun. 3, 853416 (2022)
11. Shojaeifard, A., et al.: MIMO evolution beyond 5G through reconfigurable intelligent surfaces and fluid antenna systems. Proc. IEEE 110(9), 1244–1265 (2022)
12. Paracha, K.N., Butt, A.D., Alghamdi, A.S., Babale, S.A., Soh, P.J.: Liquid metal antennas: Materials, fabrication and applications. Sensors 20, 177 (2020)
13. Huang, Y., Xing, L., Song, C., Wang, S., Elhouni, F.: Liquid antennas: Past, present and future. IEEE Open J. Antennas Propag. 2, 473–487 (2021)
14. Cetiner, B.A., Jafarkhani, H., Qian, J.-Y., Yoo, H.J., Grau, A., De Flaviis, F.: Multifunctional reconfigurable MEMS integrated antennas for adaptive MIMO systems. IEEE Commun. Mag. 42(12), 62–70 (2004)
15. Besoli, A.G., De Flaviis, F.: A multifunctional reconfigurable pixeled antenna using MEMS technology on printed circuit board. IEEE Trans. Antennas Propag. 59(12), 4413–4424 (2011)
16. Song, S., Murch, R.D.: An efficient approach for optimizing frequency reconfigurable pixel antennas using genetic algorithms. IEEE Trans. Antennas Propag. 62(2), 609–620 (2014)
17. Mitsubishi Electric: SeaAerial antenna uses seawater plume. https://www.mitsubishielectric.com
18. Hampson, M.: New antenna uses saltwater and plastic to steer radio beams. In: IEEE Spectrum-The Tech Talk blog. IEEE, Piscataway (2019)
19. Xing, L., Zhu, J., Xu, Q., Yan, D., Zhao, Y.: A circular beam-steering antenna with parasitic water reflectors. IEEE Antennas Wirel. Propag. Lett. 18(10), 2140–2144 (2019)
20. Wang, H., Shen, Y., Tong, K.F., Wong, K.K.: Continuous electrowetting surface-wave fluid antenna for mobile communications. In: Proc. IEEE Technol., Education and Netw. Conf. (TENCON 2022). IEEE, Piscataway (2022)
21. Yan, X., Li, L., Zhang, H.C., Han, J.Y.: Broadband polarization-reconfigurable liquid dielectric resonator antenna controlled by gravity. IEEE Antennas Wirel. Propag. Lett. 21(10), 2105–2109 (2022)
22. Zhang, T., Chen, Y., Yang, S.: A wideband frequency- and polarization-reconfigurable liquid metal-based spiral antenna. IEEE Antennas Wirel. Propag. Lett. 21(7), 1477–1481 (2022)
23. Geng, X., et al.: Pattern-reconfigurable liquid metal magneto-electric dipole antenna. IEEE Antennas Wirel. Propag. Lett. 21(8), 1683–1687 (2022)
24. Zhou, Y., Zhao, G., Li, X.Y., Tong, M.S.: A liquid-metal-based crossed-slot antenna with polarization and continuous-frequency reconfiguration. IEEE Open J. Antennas Propag. 3, 1102–1108 (2022)
25. Li, L., Yan, X., Zhang, H.C., Wang, Q.: Polarization- and frequency-reconfigurable patch antenna using gravity-controlled liquid metal. IEEE Trans. Circuits Syst. II Exp. Briefs 69(3), 1029–1033 (2022)
26. Martínez, J.O., et al.: Toward liquid reconfigurable antenna arrays for wireless communications. IEEE Commun. Mag. 60(12), 145–151 (2022)
27. Wong, K.K., Shojaeifard, A., Tong, K.-F., Zhang, Y.: Fluid antenna systems. IEEE Trans. Wireless Commun. 20(3), 1950–1962 (2021)
28. Chai, Z., Wong, K.K., Tong, K.F., Chen, Y., Zhang, Y.: Port selection for fluid antenna systems. IEEE Commun. Lett. 26(5), 1180–1184 (2022)
29. Wong, K.K., Shojaeifard, A., Tong, K.-F., Zhang, Y.: Performance limits of fluid antenna systems. IEEE Commun. Lett. 24(11), 2469–2472 (2020)
30. Tlebaldiyeva, L., Nauryzbayev, G., Arzykulov, S., Eltawil, A., Tsiftsis, T.: Enhancing QoS through fluid antenna systems over correlated Nakagami-m fading channels. In: Proceedings of IEEE Wireless Communications and Networking Conference (WCNC), pp. 78–83. IEEE, Piscataway (2022)
31. Psomas, C., Kraidy, G.M., Wong, K.K., Krikidis, I.: On the diversity and coded modulation design of fluid antenna systems. arXiv preprint arXiv:2205.01962 (2022)
32. Mukherjee, P., Psomas, C., Krikidis, I.: On the level crossing rate of fluid antenna systems. arXiv preprint arXiv:2205.01711 (2022)
33. Khammassi, M., Kammoun, A., Alouini, M.-S.: A new analytical approximation of the fluid antenna system channel. arXiv preprint arXiv:2203.09318 (2022)
34. Skouroumounis, C., Krikidis, I.: Fluid antenna with linear MMSE channel estimation for large-scale cellular networks. IEEE Trans. Commun. (2023)

35. Zhu, L., Ma, W., Zhang, R.: Modeling and performance analysis for movable antenna enabled wireless communications. arXiv preprint arXiv:2210.05325, 2022
36. Ma, W., Zhu, L., Zhang, R.: MIMO capacity characterization for movable antenna systems. arXiv preprint arXiv:2210.05396, 2022
37. Wong, K.K., Tong, K.F.: Fluid antenna multiple access. IEEE Trans. Wireless Commun. 21(7), 4801–4815 (2022)
38. Wong, K.K., Tong, K.F., Chen, Y., Zhang, Y.: Closed-form expressions for spatial correlation parameters for performance analysis of fluid antenna systems. IET Electron. Lett. 58(11), 454–457 (2022)
39. Wong, K.K., Tong, K.F., Chen, Y., Zhang, Y.: Fast fluid antenna multiple access enabling massive connectivity. IEEE Commun. Lett. (2023)
40. Wong, K.K., Morales-Jimenez, D., Tong, K.F., Chae, C.B.: Slow fluid antenna multiple access. IEEE Trans. Commun. (2022)
41. Choudhury, S., Gibson, J.D.: Information transmission over fading channels. In: Proceedings of IEEE Global Telecommunications Conference, pp. 3316–3321. IEEE, Piscataway (2007)
42. Stüber, G.L.: Principles of Mobile Communication, 2nd ed. Kluwer Academic Publishers, Dordrecht (2002)
43. Sklar, B.: Rayleigh fading channels in mobile digital communication systems–I: Characterization. IEEE Commun. Mag. 35(7), 90–100 (1997)
44. Beaulieu, N.C., Hemachandra, K.T.: Novel simple representations for Gaussian class multivariate distributions with generalized correlation. IEEE Trans. Inf. Theory 57(12), 8072–8083 (2011)
45. Rappaport, T.S., MacCartney, G.R., Samimi, M.K., Sun, S.: Wideband millimeter-wave propagation measurements and channel models for future wireless communication system design. IEEE Trans. Commun. 63(9), 3029–3056 (2015)
46. Hemadeh, I.A., Satyanarayana, K., El-Hajjar, M., Hanzo, L.: Millimeter-wave communications: Physical channel models, design considerations, antenna constructions, and link-budget. IEEE Commun. Surv. Tutor. 20(2), 870–913 (2018)
47. Simon, M.K.: Probability Distributions Involving Gaussian Random Variables: A Handbook for Engineers and Scientists. Springer, Boston, MA (2002)

How to cite this article: Wong, K.-K., Tong, K.-F., Chen, Y., Zhang, Y.: Maximizing the network outage rate for fast fluid antenna multiple access systems. IET Commun. , 1–12 (2023). https://doi.org/10.1049/cmu2.12592

APPENDIX A: PROOF OF THEOREM 1

Take the outage probability in (8) and write it in the form

$$p_{\text{out}}(\gamma) = \int_0^\infty \int_0^\infty e^{-z} e^{-t} \left[1 - \underbrace{\left(Q_1(\cdot,\cdot) - \cdots \right)}_{Z} \right]^N dt dz. \quad \text{(A1)}$$

The fact that the outage probability is a decreasing function of N means that $Z < 1$. Also, N should be large to reduce the outage probability to an acceptable level, which implies that Z is typically small. Hence, it is possible to approximate the outage probability by

$$p_{\text{out}}(\gamma) \approx \int_0^\infty \int_0^\infty e^{-z} e^{-t} \left[1 - N \underbrace{\left(Q_1(\cdot,\cdot) - \cdots \right)}_{Z} \right] dt dz. \quad \text{(A2)}$$

As a consequence, we can now write

$$\begin{aligned} p_{\text{out}}(\gamma) &\approx \int_0^\infty \int_0^\infty e^{-z} e^{-t}\, dt dz - NA + NB \\ &= 1 - NA + NB, \end{aligned} \quad \text{(A3)}$$

where

$$\begin{aligned} A = \int_0^\infty \int_0^\infty & e^{-z} e^{-t} \\ & \times Q_1\left(\frac{1}{\sqrt{a^2+1}} \sqrt{\frac{2\mu^2}{1-\mu^2}} \sqrt{t}, \frac{a}{\sqrt{a^2+1}} \sqrt{\frac{2\mu^2}{1-\mu^2}} \sqrt{z} \right) \\ & \times dt dz, \end{aligned} \quad \text{(A4)}$$

and

$$\begin{aligned} B = \int_0^\infty \int_0^\infty & e^{-z} e^{-t} \left(\frac{a^2}{a^2+1} \right) e^{-\frac{1}{a^2+1} \frac{\mu^2}{1-\mu^2} (a^2 z + t)} \\ & \times I_0\left(\frac{a^2}{a^2+1} \left(\frac{2\mu^2}{1-\mu^2} \right) \sqrt{zt} \right) dt dz. \end{aligned} \quad \text{(A5)}$$

First, A can be evaluated by (A6) (see top of next page) in which (a) uses Lemma 2 and (b) uses Lemma 3. Then B can be derived as (A7) (see next page) where (a) uses Lemma 1.

$$\begin{aligned} A &= \int_0^\infty e^{-z} \int_0^\infty e^{-t} Q_1\left(\frac{1}{\sqrt{a^2+1}} \sqrt{\frac{2\mu^2}{1-\mu^2}} \right. \\ &\quad \left. \times \sqrt{t}, \frac{a}{\sqrt{a^2+1}} \sqrt{\frac{2\mu^2}{1-\mu^2}} \sqrt{z} \right) dt dz \\ &\overset{(a)}{=} \int_0^\infty e^{-z} Q_1\left(0, \frac{\sqrt{2} \frac{a}{\sqrt{a^2+1}} \sqrt{\frac{2\mu^2}{1-\mu^2}} \sqrt{z}}{\sqrt{\frac{1}{a^2+1}\left(\frac{2\mu^2}{1-\mu^2} \right) + 2}} \right) dz \\ &= \int_0^\infty e^{-z} Q_1\left(0, \frac{\frac{a}{\sqrt{a^2+1}} \sqrt{\frac{2\mu^2}{1-\mu^2}}}{\sqrt{\frac{1}{a^2+1} \frac{\mu^2}{1-\mu^2} + 1}} \sqrt{z} \right) dz \end{aligned} \quad \text{(A6)}$$

$$\overset{(b)}{=}\left(\frac{2}{\frac{\frac{a^2}{a^2+1}\frac{2\mu^2}{1-\mu^2}}{\frac{1}{a^2+1}\frac{\mu^2}{1-\mu^2}+1}+2}\right)=\frac{\mu^2}{a^2+1}+1-\mu^2. \quad \text{(A6)}$$

$$\begin{aligned}B&=\left(\frac{a^2}{a^2+1}\right)\int_0^\infty e^{-z}e^{-\frac{1}{a^2+1}\left(\frac{\mu^2}{1-\mu^2}\right)a^2z}\\&\quad\times\int_0^\infty e^{-\left(\frac{1}{a^2+1}\frac{\mu^2}{1-\mu^2}+1\right)t}\\&\quad\times I_0\left(\frac{a}{a^2+1}\left(\frac{2\mu^2}{1-\mu^2}\right)\sqrt{z}\sqrt{t}\right)dtdz\\&\overset{(a)}{=}\left(\frac{a^2}{a^2+1}\right)\int_0^\infty e^{-\left[\frac{1}{a^2+1}\left(\frac{\mu^2}{1-\mu^2}\right)a^2+1\right]z}\\&\quad\times\frac{1}{\frac{1}{a^2+1}\frac{\mu^2}{1-\mu^2}+1}e^{\frac{\left(\frac{a}{a^2+1}\right)^2\left(\frac{2\mu^2}{1-\mu^2}\right)^2}{4\left(\frac{1}{a^2+1}\frac{\mu^2}{1-\mu^2}+1\right)}z}dz\\&=\left(\frac{a^2}{\frac{\mu^2}{1-\mu^2}+a^2+1}\right)\int_0^\infty e^{-\left(\frac{1}{\frac{\mu^2}{a^2+1}+1-\mu^2}\right)z}dz\\&=\frac{(1-\mu^2)a^2}{a^2+1}.\end{aligned} \quad \text{(A7)}$$

As a result, the outage probability can be found as

$$\begin{aligned}&p_{\text{out}}(\gamma)\\&\approx 1-N\times\left(\frac{\mu^2}{a^2+1}+1-\mu^2\right)+N\times\left(\frac{(1-\mu^2)a^2}{a^2+1}\right)\\&=1-\frac{N(1-\mu^2)}{a^2+1}-\frac{N\mu^2}{a^2+1}.\end{aligned} \quad \text{(A8)}$$

Finally, note that we have used the linearization $(1-Z)^N\approx 1-NZ$ for small Z and therefore, the approximation (A8) can become negative when N is extremely large. As a result, the operation $(\cdot)^+$ is adopted to guarantee positivity of the approximation, resulting in the expression (15). Moreover, we assume the small μ case and thus, we have $\mu^2\ll 1-\mu^2$ and drop the term $\frac{N\mu^2}{a^2+1}$. Last, we consider $(U-1)\gamma\gg 1$ and apply the approximation (6b) to obtain (16).